Formation and Growth of Oxide Layers at Platinum and Gold Nano- and Microelectrodes

ARTICLE *in* ANALYTICAL CHEMISTRY · SEPTEMBER 2010

Impact Factor: 5.64 · DOI: 10.1021/ac101728a · Source: PubMed

Anal. Chem. **2010,** *82,* 7135–7140

Formation and Growth of Oxide Layers at Platinum and Gold Nano- and Microelectrodes

Claudio Zuliani,[†] Darren A. Walsh,[‡] Tia E. Keyes,[†] and Robert J. Forster*,[†]

Biomedical Diagnostics Institute, Dublin City University, Dublin 9, Ireland, and School of Chemistry, University of Nottingham, Nottingham, U.K.

The construction and characterization of platinum and gold disk electrodes with minimum radii of 7 nm (platinum) and 500 nm (gold) is reported. The electrodes were prepared with a micropipet puller using a two step procedure and have been characterized using scanning electron microscopy, scanning electrochemical microscopy, high speed chronoamperometry, and cyclic voltammetry. The formation and growth of platinum and gold oxide layers, on the electrodes at time scales from microseconds to seconds, is reported. Significantly, the apparent microscopic area as determined by forming and subsequently reducing an oxide layer in acidic electrolyte using cyclic voltammetry depends dramatically on the scan rate. While conventional roughness factors between 1.8 and 3 are observed on average for scan rates above 5 V s^{-1}, the apparent roughness can exceed 30 for scan rates less than 0.5 V s^{-1}. Chronoamperometry, conducted on the microsecond to millisecond time scale, is used to probe the dynamics of monolayer and multilayer oxide formation as well as the reversibility of the oxide formation and removal. The latter study suggests that (at least for platinum) the growth of the oxide layer proceeds with a lower constant rate after an oxide monolayer is formed.

The development of reliable methods for fabricating nanometer-sized electrodes is an extremely important goal in modern electroanalytical chemistry.[1−4] The small size of nanoelectrodes, as well as their rapid response time and ability to rapidly produce steady-state currents, offers significant new opportunities in low volume analysis, high resolution imaging,[4−6] biology,[7−10] analytical chemistry,[5,11] and high speed kinetic measurements.[12−14] Several methods for fabricating nanoelectrodes have been developed including coating sharpened wires with wax[15] or electrophoretic paint[16] leaving a nanoscopic tip exposed. The two step procedure developed by Pendley et al.,[17] in which a wire is placed inside a capillary and then the assembly pulled, is a particularly useful method for fabricating nanoelectrodes.[5] This procedure has been efficiently employed in the fabrication of platinum[18−21] and, recently, of gold[22] nanoelectrodes. Using this method, Mirkin has fabricated nanoelectrodes[6,10,19,22] as small as 10 nm and used them to measure the kinetics of fast heterogeneous electron transfer for a range of redox species.[19]

A key advantage of shrinking the electrode size is that the response time decreases, allowing the dynamics of reactions to be explored over a much wider range of time scales. For example, while the impact of forming and removing an oxide layer on platinum and gold has been extensively explored,[23−27] the kinetics of the oxidation and the discrete mechanistic steps are still not fully understood.[28] Oxide formation and stripping is a particular issue for submicrometer electrodes, since surface roughness influences the overall performance of the electrode. It is thought that several anhydrous and hydrous oxide species might be involved, and it has been shown that the underlying processes

* To whom correspondence should be addressed.
[†] Dublin City University.
[‡] University of Nottingham.

(1) Heinze, H. *Angew. Chem.* **1984**, *23*, 831.
(2) Pons, S.; Fleischmann, M. *Anal. Chem.* **1987**, *59*, A1391.
(3) Forster, R. J. *Chem. Soc. Rev.* **1994**, 289.
(4) Zoski, C. G. *Electroanalysis* **2002**, *14*, 1041.
(5) Arrigan, D. W. M. *Analyst* **2004**, *129*, 1157.
(6) Sun, P.; Laforge, F. O.; Mirkin, M. V. *Phys. Chem. Chem. Phys.* **2007**, *9*, 802.
(7) Schulte, A.; Schuhmann, W. *Angew. Chem., Int. Ed.* **2007**, *46*, 8760.
(8) Adams, R. N. *Anal. Chem.* **1976**, *48*, 1126A.
(9) Roberts, W. S.; Lonsdale, D. J.; Griffiths, J.; Higson, S. P. J. *Biosens. Bioelectron.* **2007**, *23*, 301.
(10) Sun, P.; Laforge, O.; Abeyweera, T. P.; Rotenberg, S. A.; Carpino, J.; Mirkin, M. *Proc. Natl. Acad. Sci. U.S.A.* **2008**, *105*, 443.
(11) Watkins, J. J.; Chen, J.; White, H. S.; Abruna, H. D.; Maisonhaute, E.; Amatore, C. *Anal. Chem.* **2003**, *75*, 3962.
(12) Forster, R. J.; Loughman, P.; Keyes, T. E. *J. Am. Chem. Soc.* **2000**, *122*, 11948.
(13) Forster, R. J. *Langmuir* **1995**, *11*, 2247.
(14) Forster, R. J.; Keyes, T. E. Microelectrode Applications. In *Handbook of Electrochemistry*; Zoski, C. G., Ed.; Elsevier: Netherlands, 2007; pp 171.
(15) Mirkin, M. V.; Fan, F. F.; Bard, A. J. *J. Electroanal. Chem.* **1992**, *328*, 47.
(16) Tel-Vered, R.; Walsh, D. A.; Mehrgardi, M. A.; Bard, A. J. *Anal. Chem.* **2006**, *78*, 6959.
(17) Pendley, B. D.; Abruna, H. D. *Anal. Chem.* **1990**, *62*, 782.
(18) Shao, Y.; Mirkin, M. V. *Anal. Chem.* **1997**, *69*, 1627.
(19) Sun, P.; Mirkin, M. V. *Anal. Chem.* **2006**, *78*, 6526.
(20) Katemann, B. B.; Schuhmann, W. *Electroanalysis* **2002**, *14*, 22.
(21) Ufheil, J.; Heb, C.; Borgwarth, K.; Heinze, J. *Phys. Chem. Chem. Phys.* **2005**, *7*, 3185.
(22) Velmurugan, J.; Sun, P.; Mirkin, M. V. *J. Phys. Chem. C.* **2009**, *113*, 459.
(23) Schneeweiss, M. A.; Kolb, D. M.; Liu, D. Z.; Mandler, D. *Can. J. Chem.* **1997**, *75*, 1703.
(24) Schneeweiss, M. A.; Kolb, D. M. *Solid State Ionics* **1997**, *94*, 171.
(25) Hirai, N.; Watanabe, K.; Hara, S. *Surf. Sci.* **2001**, *493*, 568.
(26) Hirai, N.; Yamauchi, M.; Tanaka, T.; Hara, S. *Sci. Technol. Adv. Mater.* **2004**, *5*, 115.
(27) Nishizawa, T.; Nakada, T.; Kinoshita, Y.; Miyashita, S.; Sazaki, G.; Komatsu, H. *Surf. Sci.* **1996**, *367*, L73.
(28) Jerkiewicz, G.; Vatankhah, G.; Lessard, J.; Soriaga, M. P.; Park, Y. *Electrochim. Acta* **2004**, *49*, 1451.

10.1021/ac101728a
Published on Web 08/05/2010

depend on the sample pretreatment.[29−33] In particular, platinum and gold oxides seem to possess a two layer-structure. For the innermost oxide layer, place exchange of the surface atoms may occur during the metal oxidation which leads to a quasi 3D surface lattice.[28,34−36] The inner layer is associated with a lower oxidation state of the metal and its growth is limited by the interfacial place exchange.[34−39] However, the outer oxide film (associated with a higher oxidation state of the metal) grows without reaching any limit up to some 100 equivalent monolayers,[35,36] e.g., high surface areas have been associated with the reduction of the platinum β-oxide film.[39] When the oxide coverage is less than a monolayer, the growth rate follows a logarithmic rate law. In contrast, for oxide layers greater than about 1 monolayer, an inverse-logarithm rate law is followed. Moreover, for thicker layers, the rate is limited by the rate of escape of the metal cation into the oxide at the inner metal/oxide interface.[35,36] Here, we exploit the fast response time of the microelectrodes to probe the kinetics of oxide layer growth on platinum over a wide time domain.

EXPERIMENTAL SECTION

Chemicals, Materials, and Equipment. Cyclic voltammetry and scanning electrochemical microscopy (SECM) were performed using the CHI900A Scanning Electrochemical Microscope. A custom built programmable function generator−potentiostat[40] was used to carry out short time scale chronoamperometry. Unless stated otherwise, all the potentials reported are against a custom-made Ag/AgCl (saturated KCl) reference electrode (−0.045 V vs SCE). A platinum wire was employed as the counter electrode, and a platinum disk electrode with a radius of 1 mm was used as a substrate in the SECM measurements. To speed up the operations during an SECM approach, a long-distance microscope helped in positioning the probe quite close to the substrate, i.e., ∼50−100 μm away from the surface. A Nikon ECLIPSE ME600D microscope was employed in the preliminary evaluation of the pulling step. Ferrocenemethanol and potassium chloride were purchased from Sigma-Aldrich while ruthenium(III) hexamine chloride was from Strem Chemicals, and they were used as received. All the aqueous solutions were prepared from Milli-Q reagent water (Millipore Corp.), 18 MΩ cm. All the experiments were conducted at room temperature 20 ± 2 °C.

Microelectrodes were fabricated using the Sutter P-2000 laser puller. The barrels used were borosilicate (0.50 mm inner diameter (i.d.); 1.00 mm outer diameter (o.d.); 10 cm long and 0.3 mm i.d.; 1.00 mm o.d.; 7.5 cm long); aluminosilicate (0.68 mm i.d.; 1.00 mm o.d.; 10 cm long); as well as quartz: (0.5 mm i.d.; 1.00 mm o.d.; 7.5 cm long and 0.30 mm i.d.; 1.00 mm o.d.; 7.5 cm long). All the capillaries were supplied by Sutter Instruments. The 12.5 μm hard temper gold and 12.5 μm annealed platinum wires employed in the microelectrode fabrication were purchased from Goodfellow Cambridge Limited. A pump (N810.3FT.18, KNF Laboport) and flexible silicone tubing (Cole Parmer) were employed in the sealing step. Electrodes were bevelled using the Sutter BV-10 beveller. A 25 W mini-drill (Radionics), held at an angle of 45° from the plane of the grinding disk, was employed when sharpening of the electrodes was required. The rotation speed was kept between 200 and 300 rpm using a variable power supply. The standard grinding disk provided by Sutter Instruments or alumina sheet (30, 15, 5, 3, 1, and 0.3 μm, Thorlabs) mounted on the top of the grinding disk of the beveller was used in the polishing and sharpening steps.

Characterization. The capacitive contribution was calculated from the voltammogram by measuring the difference in current between the forward and backward scans in a nonfaradic region (Δi) as a function of the scan rate (v). The slope of this plot[42] is given by 2AC, where A is the electrode area and C is the interfacial capacitance and allows the capacitance to be determined. The experimental SECM approach curves were fitted to the expressions elaborated by Lefrou[43] and Cornut et al.,[44] respectively, for the positive and negative feedback. The R_G factor (ratio between the glass shield and the electrode radii) was calculated by fitting the SECM approach curve under conditions of negative feedback. This factor is an average value as an uncentered electrode and has a smaller apparent R_G.[45] The roughness factor, ρ, of the electrodes was determined by cycling the potential between the oxygen and the hydrogen evolution regimes in 1 M H_2SO_4 (99.999%) that was thoroughly deoxygenated with N_2.[46] The values of 420 and 390 μC cm^{-2} were used as reference charge for reduction of an oxide monolayer on polycrystalline platinum and gold, respectively.[46] Cell time constants (RC) were determined from a plot of the logarithm of the capacitive current against time following a potential step.[42]

Electrode Preparation. The capillaries were mounted in the laser puller; a vacuum was attached to both ends, and a stopper was applied to prevent the hard pull. The following programs were used to seal the platinum wire within 0.3 and 0.5 mm i.d. capillaries.

Program 1: HEAT: 795 ± 10; FIL: 5; VEL: 255; DELAY: 255; PULL: 0.

Program 2: HEAT: 730 ± 10; FIL: 5; VEL: 255; DELAY: 255; PULL: 0.

Each program ran for 40 s and, after a pause of 20 s, was repeated. A total of four and three heating/cooling cycles were

(29) Zhang, Y.; Gao, X.; Weaver, M. J. *J. Phys. Chem.* **1993**, *97*, 8656.
(30) Burke, L. D.; O'Mullane, A. P. *J. Solid State Electrochem.* **2000**, *4*, 285.
(31) Burke, L. D.; Lee, B. H. *J. Electroanal. Chem.* **1992**, *330*, 637.
(32) Burke, L. D.; O'Sullivan, J. F. *J. Electroanal. Chem.* **1990**, *285*, 195.
(33) Hamelin, A. *J. Electroanal. Chem.* **1996**, *407*, 1.
(34) Alsabet, M.; Grden, M.; Jerkiewicz, G. *J. Electroanal. Chem.* **2006**, *589*, 120.
(35) Tremiliosi-Filho, G.; Dall'Antonia, L. H.; Jerkiewicz, G. *J. Electroanal. Chem.* **1997**, *422*, 149.
(36) Tremiliosi-Filho, G.; Dall'Antonia, L. H.; Jerkiewicz, G. *J. Electroanal. Chem.* **2005**, *578*, 1.
(37) Tremiliosi-Filho, G.; Jerkiewicz, G.; Conway, B. E. *Langmuir* **1992**, *8*, 658.
(38) Conway, B. E.; Tremiliosi-Filho, G.; Jerkiewicz, G. *J. Electroanal. Chem.* **1991**, *297*, 435.
(39) Farebrother, M.; Goledzinowski, M.; Thomas, G.; Birss, V. I. *J. Electroanal. Chem.* **1991**, *297*, 469.
(40) Forster, R. J.; Faulkner, L. R. *J. Am. Chem. Soc.* **1994**, *116*, 5444.
(41) Jose, B.; Steffan, R.; Neugebauer, U.; Sheridan, E.; Marthi, R. F.; Forster, R. J.; Keyes, T. E. *Phys. Chem. Chem. Phys.* **2009**, *11*, 10923.
(42) Bard, A. J.; Faulkner, L. R. Double-Layer Capacitance and Charging Current in Electrochemical Measurements. In *Electrochemical Methods. Fundamentals and Applications*; John Wiley and Sons, Inc: Hoboken, NJ, 2001; pp 14.
(43) Lefrou, C. *J. Electroanal. Chem.* **2006**, *592*, 103.
(44) Cornut, R.; Lefrou, C. *J. Electroanal. Chem.* **2007**, *604*, 91.
(45) Cornut, R.; Lefrou, C. In *3D Steady-state Simulations of Scanning Electrochemical Microscopy Experiments with Microdisk Electrode*; Excerpt from the Proceedings of the COMSOL Users Conference, Grenoble, 2007.
(46) Bard, A. J.; Faulkner, L. R. Microscopic and Geometric Areas. In *Electrochemical Methods. Fundamentals and Applications*; John Wiley and Sons, Inc: Hoboken, NJ, 2001; pp 166.

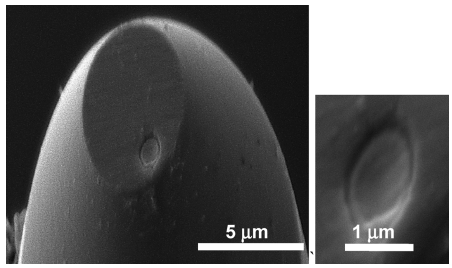

Figure 1. SEM pictures of a platinum microelectrode with radius of approximately of 500 nm (A) at low magnification and (B) at high magnification. The accelerating voltage is 5 kV.

performed in the case of Programs 1 and 2, respectively. The vacuum tubes and the stoppers were then removed, and after a minute pause, the capillary was pulled according to

Program 3: HEAT: 710 ± 20; FIL: 1 ± 1; VEL: 43 ± 2; DELAY: 124 ± 3; PULL: 120 ± 60.

Quartz is an excellent insulation material, and it was preferred to borosilicate in the preparation of platinum probes because it shows superior flexibility and strength than other glasses.[47]

For the gold probes, different programs have been set depending on the glass types (soda, borosilicate, aluminosilicate) and sizes employed. The best results were obtained with 0.3 mm i.d. borosilicate, following Programs 4 and 5:

Program 4: HEAT: 315 ± 5; FIL: 5; VEL: 255; DELAY: 255; PULL: 0.

Program 5: HEAT: 330 ± 10; FIL: 0−1; VEL: 32 ± 1; DELAY: 126 ± 2; PULL: 160 ± 40.

Program 4 ran for 40 s, followed by a pause of 20 s. A total of four heating/cooling cycles were performed. The vacuum tubes and the stoppers were then removed, and after a minute pause, the capillary was pulled according to Program 5, which pulled the capillaries apart in ∼4.0−4.5 s.

Copper enameled wire (0.2 mm, Rowan Cable Products LTD) was inserted along with a 2 to 3 mm long piece of low melting point solder (32 swg, Combine Precision Components). Then, an electrical contact is achieved by melting the solder using a heat gun. The copper cable was fixed to the top of the capillary with Araldite glue (Bostik).

RESULTS AND DISCUSSION

General Properties. Figure 1 shows a typical scanning electron microscopy (SEM) image of a platinum microelectrode formed by simultaneously sealing and stretching a 12.5 μm annealed platinum wire in quartz glass. This image reveals that the radius of the electrode is approximately 500 nm. The platinum wire is sealed somewhat off-center, and the active electrode shows some elliptical character. However, there is no evidence of defects in the seal between the glass and platinum wire. The percentage of successful platinum probes with radii smaller than 100 nm is approximately 20% while approximately 60% have radii between 100 and 1000 nm and 10% have radii in the micrometer range. Gold microelectrodes have a lower overall percentage of successful pulls, approximately 60%, with only 10% of the electrodes having submicrometer radii, but none are smaller than 500 nm.

Electrochemical Properties. Cyclic voltammograms obtained with these electrodes using a solution phase redox probe, such

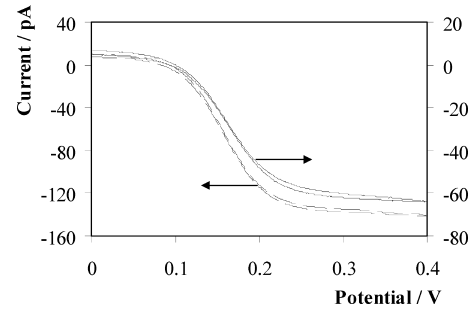

Figure 2. Cyclic voltammetry responses for (—) 225 nm platinum and (- - -) 520 nm diameter gold probes in a solution of 1.033 mM FcMeOH in aqueous 0.1 M KCl. The potential was swept between 0.0 and 0.4 V vs Ag/AgCl at a scan rate of 5 mV s^{-1}.

as ferrocenemethanol, are consistent with the response expected for an electrochemical reaction involving a solution phase reactant under radial diffusion control. As illustrated in Figure 2, well-defined steady state currents are observed and there is little hysteresis between the forward and backward scans. Moreover, there is no significant slope to the capacitive current observed away from E°□. These observations suggest that a high quality seal is formed between the platinum wire and the surrounding glass.[3,48] Significantly, the radius measured from the limiting current is indistinguishable from that obtained using SEM. One advantage of these nanodimensioned electrodes is that it is possible to increase the scan rate while maintaining radial diffusion control. For example, the voltammetric response of the 520 nm diameter gold electrode is controlled by radial diffusion for scan rates of several thousand volts per second.

SECM has become an essential technique in the protocol for the characterization of nanoelectrodes to determine their geometry, e.g., recess.[18,19] However, as the electrode size is decreased, SECM becomes increasingly challenging as the tip to substrate alignment is not trivial and it may be responsible for approach curves with low feedback current.[10,49,50] Figure 3 shows that good agreement is observed between the experimental and the fitted curves over insulating (lower curve) and conducting (upper curve) substrates. It can be seen that the tip can approach the substrate up to values of the absolute distance, $L(d/a)$, lower than 1, which indicates that the disk surface is not significantly recessed. However, approach curves with electrodes smaller than 100 nm show lower feedback currents, most probably because of the tip to substrate misalignment. It is important to note that this issue has been effectively addressed by Mirkin and co-workers who have demonstrated approach curves with feedback current ratios equal to 8 and above.[19,22,51] Despite the lower feedback current ratios of this work, it was possible to image an array of 640 nm diameter gold nanocavities[41,52] by using the feedback mode using a probe of approximately 180 nm.

Oxide Formation and Growth. A key challenge in fabricating nanometer dimensioned electrodes is the production of surfaces

(47) Levis, R. A.; Rae, J. L. *Biophys. J.* **1993**, *65*, 1666.
(48) Forster, R. J. Microelectrodes-Retrospect and Prospect. In *Encyclopedia of electrochemistry. Vol. 3. Instrumentation and electroanalytical chemistry*; Unwin, P. R., Ed.; Wiley Ltd: Federal Republic of Germany, 2003; pp 160.
(49) Sun, P.; Mirkin, M. V. *J. Am. Chem. Soc.* **2008**, *130*, 8241.
(50) Katemann, B. B.; Schulte, A.; Schuhmann, W. *Electroanalysis* **2004**, *16*, 60.
(51) Sun, P.; Mirkin, M. V. *Anal. Chem.* **2007**, *79*, 5809.
(52) Mallon, C. T.; Jose, B.; Forster, R. J.; Keyes, T. E. *Chem. Commun.* **2010**, *46*, 106.

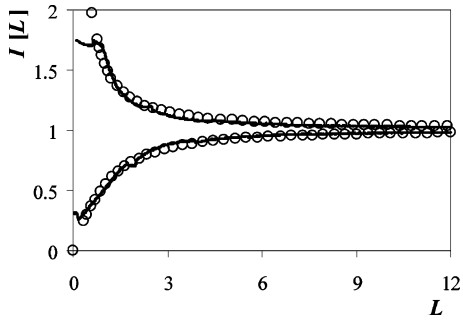

Figure 3. Positive (upper curve) and negative (lower curve) feedback approach curves obtained during the reduction of $[Ru(NH_3)_6]^{3+}$ as the SECM tip approaches platinum and Teflon substrates, respectively. The SECM tip was a 530 nm platinum electrode, and it was immersed in a solution of 10 mM $[Ru(NH_3)_6]Cl_3$ in aqueous 0.1 M KCl. The probe potential was held at −0.3 V vs Ag/AgCl to drive the reduction of $[Ru(NH_3)_6]^{3+}$ at the diffusion controlled rate. The solid lines (—) represent the experimental data while the circles (○) represent the theoretical curves for inlaid disk electrodes with a radius of 530 nm and R_G value of 7. The tip approach speed was 40 nm s^{-1}.

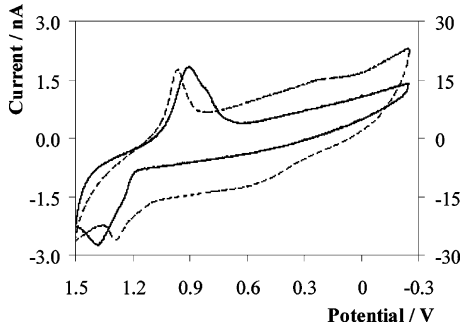

Figure 4. Cyclic voltammetry of a 5.2 μm radius gold inlaid disk electrode immersed in 1 M H_2SO_4 aqueous solution. The voltammograms were recorded at the scan rate of (- - -) 0.1 V s^{-1} (scale to the left) and (—) 5 V s^{-1} (scale to the right).

with reasonable roughness factors (ideally less than 2), as given by the ratio of the microscopic to geometric areas. Voltammetry in 1 M H_2SO_4 was used to calculate the electrochemical area of both the platinum and gold electrodes. In all cases, the number of voltammetric cycles was minimized so as to avoid roughening of the electrode surface. Figure 4 shows the voltammograms obtained at 0.1 and 5 V s^{-1} for a 5.2 μm radius gold microelectrode. At 0.1 V s^{-1}, the metal oxide reduction peak is well-defined and it is centered at 0.95 V, but on increasing the scan rate, it shifts toward more negative potential and it broadens. The microscopic area of the electrode was determined from the charge passed under the oxide reduction peak (390 μC cm^{-2}). Voltammetry of platinum microelectrodes in 1 M H_2SO_4 at a high scan rate show well-defined metal oxide reduction at approximately 0.45 V and well-defined hydrogen adsorption and desorption peaks, suggesting a clean surface. However, the voltammetric response changes significantly as the scan rate is decreased, i.e., the oxide reduction peak broadens and the hydrogen adsorption/desorption peaks become significantly less well-defined. The microscopic area was determined from the charge passed under either the hydrogen adsorption/desorption peaks (210 μC cm^{-2}) or the oxide reduction peak (420 μC cm^{-2}). Taking into account the geometric areas determined using SEM images or the steady

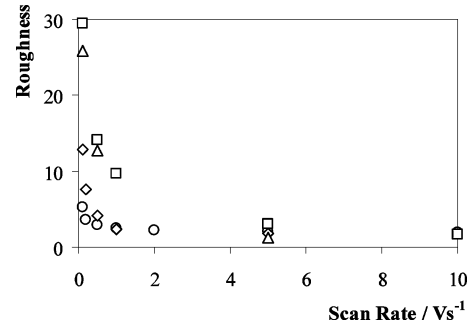

Figure 5. Roughness factors calculated for gold and platinum microelectrode from the charge passed under the metal reduction peak in function of the scan rate. The electrodes were immersed in 1 M H_2SO_4, and the potential was swept between −0.250 and 1.500 V in case of gold UMEs or between −0.2 and 1.35 V in case of platinum UMEs. (○) 5.2 μm gold, (□) 4.8 μm gold, (Δ) 2.6 μm platinum, and (◊) 3.7 μm platinum electrodes.

state current, the surface roughness of gold and platinum ultramicroelectrodes (UMEs) evaluated from cyclic voltammograms (CVs) in 1.0 M H_2SO_4 at 5 V s^{-1} is between 1.2 and 3. However, Figure 5 shows that, significantly, the apparent roughness factors obtained are strikingly large with values up to 30 being observed when the experimental scan rate is decreased to 0.1 V s^{-1}. No correlation between the roughness factor and the size of the probes was observed. While a parasitic Faradaic process from low concentrations of adventitious impurities in solution may contribute to the observed response, they are unlikely to dominate. Also, an imperfect seal between the metal wire and the glass body could increase the area available for oxide formation. However, the observation of a well-defined steady state current, low capacitance, small *RC*, and consistency of the electrode areas, as determined using SEM and fast scan voltammetry, suggest that poor sealing is not the origin of the large apparent roughness measured at slow scan rates. Gold and platinum dissolution during the reductive sweep has also been reported in the literature[53] but, in the experimental conditions of this work, it should not be responsible for the high apparent roughness factor at slow scan rates.[34,38]

It appears that under slow scan conditions, more than a monolayer of metal oxide may form, and potential step chronoamperometry has been used to explore this behavior in more detail. Chronoamperometry is superior to voltammetry in this context since the potential can be abruptly stepped to a constant value, e.g., to a value where an oxide monolayer is formed, and the state of the electrode is not the result of several processes, each occurring at a different potential. Moreover, previous work has shown that oxide coverages greater than a monolayer can be created if the electrode is held at a positive potential for extended times.[28,36] The dynamics of oxide formation has been extensively studied, and these results suggest that upon initial oxidation a hydrous oxide is formed at submonolayer to monolayer coverages that reorganizes by a place-exchange mechanism between the surface oxygens and the underlying platinum atoms. However, the reversibility of the initial coating and the dynamics of its formation and subsequent reorganization have largely been restricted to relatively long time scales. Here, we report on the use of chronoamperometry conducted on the microsecond time

(53) Cadle, S. H.; Bruckenstein, S. *Anal. Chem.* **1974**, *46*, 16.

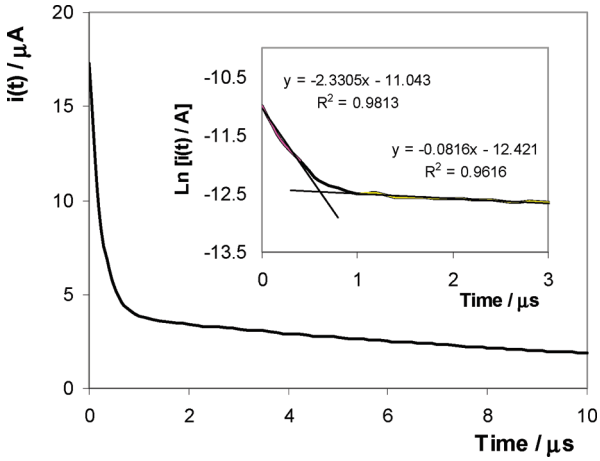

Figure 6. Short time scale current−time response for a 2 μm radius platinum microelectrode following a potential step from 0.000 to +1.200 V in 0.1 M H_2SO_4 as supporting electrolyte. The inset shows the semilog current vs time plot.

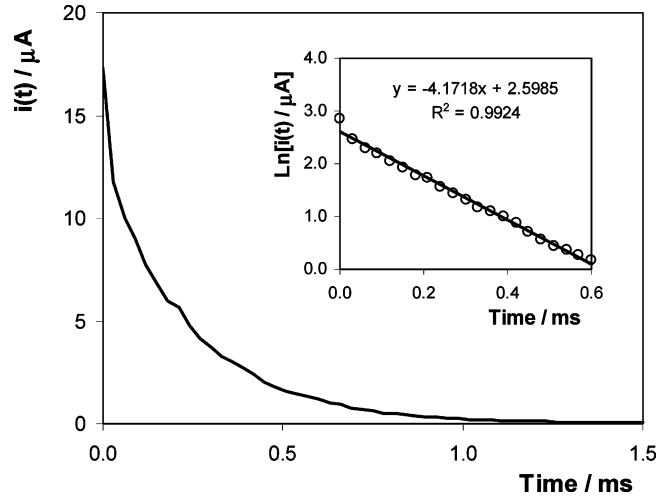

Figure 7. Long time scale current−time response for a 2 μm radius platinum microelectrode following a potential step from 0.000 to +1.200 V in 0.1 M H_2SO_4 as supporting electrolyte. The inset shows the semilog current vs time plot.

scale to probe the platinum oxidation processes. Thus, the oxide can be studied before it has significant time to undergo place exchange. First, we report on the dynamics and reversibility of the formation of the initial oxide coating. Second, the kinetics of place exchange or cation extraction that can lead to multiple monolayers and, hence, very large apparent surface roughnesses are considered.

Figure 6 shows the current−time response for a 2 μm radius platinum microelectrode following a potential step from 0.000 to +1.200 V in 0.1 M H_2SO_4 as supporting electrolyte. At short times, the current response is dominated by double layer charging and can be described by eq 1:

$$i_C(t) = \Delta E/R\exp(-t/RC) \quad (1)$$

where ΔE is the pulse amplitude, R is the total cell resistance, and C is the double layer capacitance. The inset of Figure 6 represents the semilog current vs time plot which shows that an approximately linear response is observed for times shorter than approximately 400 ns. The intercept and slope of the best fit line to these data yield resistance and capacitance values of approximately 63 ± 10 kΩ and 6.8 ± 0.4 pF, respectively. These values yield an RC time constant for the electrode of 425 ± 55 ns, demonstrating the ability of these small probes to respond quickly to changes in the applied potential. At longer times, the current is dominated by oxidation of the platinum surface. The linearity of the semilog plot for times longer than 400 ns suggests that under these conditions the current response can be adequately described according to first order kinetics:

$$i_{Ox,\,mono}(t) = k_{Ox,\,mono}Q_{Ox,\,mono} \times \exp(-k_{Ox,\,mono}t) \quad (2)$$

where $k_{Ox,\,mono}$ is the rate constant for monolayer oxide formation and $Q_{Ox,\,mono}$ is the charge passed. The best fit line to the longer time data indicates that the rate for submonolayer to monolayer oxide formation is $7.5 \pm 0.6 \times 10^4$ s^{-1}. Significantly, the charge passed is $5.3 \pm 0.3 \times 10^{-11}$ C. Given that the charge associated with the formation of an oxide monolayer on polycrystalline platinum is 420 μC cm^{-2}, this corresponds to formation of a dense oxide monolayer and there is no evidence of place exchange or multiple oxide layers being formed at these short time scales. The reversibility of this oxide monolayer formation was probed by measuring the charge, $Q_{Red,mono}$, following a potential step to +0.300 V, i.e., a step to the foot of the oxide reduction peak but more positive than the double layer region, so as to drive reduction of the oxide. The ratio $Q_{Ox,mono}/Q_{Red,\,mono}$ is 1.1 ± 0.1 where oxidation is allowed to proceed for up to 10 μs. This result indicates that, where the oxidation charge passed does not exceed that associated with the formation of an oxide monolayer, this process is reversible without the application of a large driving force.

Significantly, Figure 6 shows that the current following a step to +1.100 V does not decay to zero within 10 μs but persists for longer times. Figure 7 shows that the current associated with platinum oxidation decays to approximately zero at times on the order of 1.5 ms. The oxidation rate as determined from the slope of the semilog plot is $4.2 \pm 0.3 \times 10^2$ s^{-1}, and the charge passed, $1.7 \pm 0.2 \times 10^{-9}$ C, is equivalent to that associated with more than 30 oxide monolayers. Therefore, consistent with the slow scan rate cyclic voltammetry data, it appears that thick oxide layers can be formed on these microelectrodes most likely by a high field growth mechanism. Significantly, this oxide cannot be removed by stepping the potential to +0.300 V, e.g., approximately 5% of the oxidation charge passed during a 30 ms step to +1.100 V is recovered during a 10 s reducing step to +0.300 V. This result confirms that these thick oxide films have a significant degree of irreversibility. However, stepping the potential into the double layer region for 1−5 s recovers >90% of the charge passed during oxidation, suggesting complete reduction of the thick oxide coating at long times.

These data indicate that oxide monolayer formation at +1.100 V proceeds rapidly, half-life of approximately 10 μs, and reversibly. Thicker oxide layers, up to 30 equivalent monolayers, can be formed by prolonged oxidation. These results highlight the need to carefully select the scan rate in voltammetry if the correct

surface roughness values are to be measured and restructuring of the surface avoided.

CONCLUSIONS

Inlaid disk platinum nanoelectrodes with radius smaller than 1 μm and gold ultramicroelectrodes have been prepared by sealing metal microwires in glass and pulling using a laser puller, as described previously.[18−20] The nanoelectrodes were characterized using SEM, CV, and SECM. The formation and growth of metal oxide layers in sulfuric acid media was investigated by CV and high speed chronoamperometry. Significantly, it is found that, both for platinum and gold, the roughness factor depends on the experimental scan rate and that the growth of platinum oxide proceeds with a slower constant rate after the monolayer formation. The latter behavior is not fully understood, but it possibly arises from the enhanced oxygen diffusion at UMEs which may affect the place exchange mechanism of the oxide formation.

ACKNOWLEDGMENT

We appreciate the ongoing financial support from Science Foundation Ireland under the Biomedical Diagnostics Institute (Award No. 05/CE3/B754).

Received for review February 24, 2010. Accepted July 19, 2010.

AC101728A